A mutation in the nucleoporin-107 gene causes XX gonadal dysgenesis

Ariella Weinberg-Shukron,[1,2] Paul Renbaum,[1] Rachel Kalifa,[3] Sharon Zeligson,[1] Ziva Ben-Neriah,[4] Amatzia Dreifuss,[3] Amal Abu-Rayyan,[5] Noa Maatuk,[6] Nilly Fardian,[3] Dina Rekler,[3] Moien Kanaan,[5] Abraham O. Samson,[6] Ephrat Levy-Lahad,[1,2] Offer Gerlitz,[3] and David Zangen[7]

[1]Medical Genetics Institute, Shaare Zedek Medical Center, Jerusalem, Israel. [2]Hebrew University, Hadassah Medical School, Jerusalem, Israel. [3]Department of Developmental Biology and Cancer Research, Institute for Medical Research Israel-Canada, Hebrew University, Faculty of Medicine, Jerusalem, Israel. [4]Genetic Clinic, Hadassah Medical Center, Jerusalem, Israel. [5]Hereditary Research Laboratory, Bethlehem University, Bethlehem, Palestine. [6]Faculty of Medicine in the Galilee, Bar-Ilan University, Safed, Israel. [7]Division of Pediatric Endocrinology, Hadassah Hebrew University Medical Center, Jerusalem, Israel.

Ovarian development and maintenance are poorly understood; however, diseases that affect these processes can offer insights into the underlying mechanisms. XX female gonadal dysgenesis (XX-GD) is a rare, genetically heterogeneous disorder that is characterized by underdeveloped, dysfunctional ovaries, with subsequent lack of spontaneous pubertal development, primary amenorrhea, uterine hypoplasia, and hypergonadotropic hypogonadism. Here, we report an extended consanguineous family of Palestinian origin, in which 4 females exhibited XX-GD. Using homozygosity mapping and whole-exome sequencing, we identified a recessive missense mutation in nucleoporin-107 (*NUP107*, c.1339G>A, p.D447N). This mutation segregated with the XX-GD phenotype and was not present in available databases or in 150 healthy ethnically matched controls. NUP107 is a component of the nuclear pore complex, and the NUP107-associated protein SEH1 is required for oogenesis in *Drosophila*. In *Drosophila*, Nup107 knockdown in somatic gonadal cells resulted in female sterility, whereas males were fully fertile. Transgenic rescue of *Drosophila* females bearing the Nup107^{D364N} mutation, which corresponds to the human NUP107 (p.D447N), resulted in almost complete sterility, with a marked reduction in progeny, morphologically aberrant eggshells, and disintegrating egg chambers, indicating defective oogenesis. These results indicate a pivotal role for NUP107 in ovarian development and suggest that nucleoporin defects may play a role in milder and more common conditions such as premature ovarian failure.

Introduction

XX female gonadal dysgenesis (XX-GD) is characterized by lack of spontaneous pubertal development, primary amenorrhea, uterine hypoplasia, and hypergonadotropic hypogonadism as a result of streak gonads. XX disorders of sexual development (XX-DSD) are infrequent (1), and (46-XX) females with isolated hypergonadotropic ovarian dysgenesis (MIM #233300) constitute a rare, genetically heterogeneous condition. In recent years, XX-DSD with ovarian dysgenesis have been shown to be caused by autosomal recessive mutations in the genes encoding the follicle-stimulating hormone (*FSH*) receptor, *WNT4* (2, 3), *R-spondin* (4, 5), *PSMC3IP* (6), *MCM9* (7), *MCM8* (8, 9), *STAG3* (10), and *SYCE1* (11) or by X-linked recessive mutations in *BMP15* (12, 13). These and other studies indicate that ovarian development is an active process involving signaling pathways and crosstalk between somatic and germ cells and not simply a passive process unfolding in the absence of *SRY*, the testis determining gene on the Y chromosome (14). Nevertheless, delineation of the downstream signaling cascade(s) orchestrating ovarian development remains rudimentary, particularly compared with the knowledge gained over the last 25 years about the major genes determining male differentiation pathway (e.g., *SRY*, *SOX9*). Identification of new genes underlying XX-GD has been hampered, even in the era of genomic sequencing, by the combination of significant genetic heterogeneity and the paucity of families with multiple affected individuals.

In humans, ovarian morphogenesis is tightly linked to oogenesis and folliculogenesis. Oogenesis begins in the fetal ovaries early in fetal development, when primordial germ cells become oogonia and then, following rapid mitotic proliferation, oogonia enter meiosis to become oocytes. Folliculogenesis begins in the latter half of fetal development, when oocytes are individually surrounded by squamous pregranulosa cells. The follicle is the basic unit of the ovary, in which oocytes are ultimately encased by granulosa cells and supported by theca cells in the mesenchyme. Granulosa cells, which later become cumulus cells, act as "nurse" cells, and theca cells provide the necessary estrogenic precursor, androstenedione. At birth, human ovaries contain approximately 1 to 2 million nongrowing, preantral follicles, containing oocytes arrested in meiosis I. From puberty to menopause, FSH promotes further granulosa cell proliferation and follicular development, and the

▶ Related Commentary: p. 4005

Authorship note: Paul Renbaum and Rachel Kalifa, as well as Offer Gerlitz and David Zangen, contributed equally to this work.
Conflict of interest: The authors have declared that no conflict of interest exists.
Submitted: July 6, 2015; **Accepted:** September 3, 2015.
Reference information: *J Clin Invest*. 2015;125(11):4295–4304. doi:10.1172/JCI83553.

periodic rise in luteinizing hormone (LH) results in ovulation of the dominant follicle, which is accompanied by completion of meiosis I and arrest at meiosis II until fertilization (15). The follicular microenvironment, which is critical for oogenesis and ovulation, is formed through complex intercellular communication and signaling pathways. Perturbations in any of these processes can result in impaired development, physiology, and survival of oocytes, as reflected by genes known to be mutated in XX-GD. For example, the FSH receptor is required for granulosa cell response to *FSH*; *BMP15*, a member of the TGF-β superfamily, is critical for multiple aspects of folliculogenesis and oocyte developmental competence (reviewed in ref. 16); *STAG3*, a cohesin subunit, and *SYCE1*, a synaptonemal complex protein, are required for chromosomal segregation in meiosis (10, 17); and *MCM8* and *MCM9* are necessary for meiotic homologous recombination (18).

In *Drosophila*, each adult ovary consists of 15 to 20 parallel ovarioles, which contain a series of sequentially developing follicles called egg chambers (reviewed in refs. 19, 20). Each *Drosophila* oocyte develops within an egg chamber that contains both germ cells and somatic cells. Somatic follicle cells surround the egg chamber, providing the proper environment for the development of 16 germ cells within. One of these cells is specified to become the oocyte and initiates meiosis. The remaining 15 germ cells differentiate as nurse cells, large polyploid cells that synthesize RNA, proteins, and organelles destined for the oocyte. Individual egg chambers progress through 14 defined stages (19). The oocyte and nurse cells remain similar in size until stage 8, at which point the oocyte begins to increase markedly in volume with the onset of vitellogenesis (yolk protein synthesis and uptake). The follicle cells synthesize and secrete proteins to generate the vitelline membrane and chorion that surround the fully developed oocyte.

Drosophila has proved to be a useful model for human ovarian dysfunction in which orthologous genes exist. Examples include the cytokinesis gene *DIAPH2*, whose disruption by a balanced X;12 translocation in a family with premature ovarian failure (MIM #300511) (21) is echoed by female sterility in the *Drosophila* mutant for the orthologous gene *dia* (22). In addition, the *Drosophila* decapentaplegic (*Dpp*) gene, which is a TGF-β superfamily ligand and a functional ortholog of mammalian *BMP* genes, acts as a local niche signal whose activity is permissive for germline stem cell maintenance in the ovary (23).

In this study, using homozygosity mapping and whole-exome sequencing, we identified a missense mutation in the ubiquitously expressed and essential nuclear pore complex (NPC) gene, nucleoporin-107 (*NUP107*, c.1339G>A, p.D447N), as the genetic basis for XX-GD in 4 females from a consanguineous family. Modeling this mutation in *Drosophila* female flies resulted in defective oogenesis and female infertility, thus demonstrating the tissue-specific importance of *Nup107* for ovarian development and function.

Results

Patients and clinical analysis

Family A is an extended, highly consanguineous family of Palestinian origin. The proband (IV-5, Figure 1A), a daughter of first cousin parents, was diagnosed with XX ovarian dysgenesis after presenting at 15 years of age with absence of spontaneous pubertal development, minimal breast development, pubertal hair at Tanner stage II, primary amenorrhea, and hypergonadotrophic hypogonadism (LH level of 52 IU/l and FSH level of 87 IU/l). Imaging studies (ultrasound and MRI) indicated the presence of a relatively small uterus (length of 4 cm), and ovaries were not detected. She responded well to hormone replacement therapy, and after 24 months of treatment, she achieved mean familial height (158 cm), secondary sexual characteristics, and regular periods. Following her diagnosis, we identified very similar clinical features in her younger sister (IV-6, Figure 1A) and several of her first cousins (IV-1 and IV-7, Figure 1A). All affected individuals had an absence of spontaneous pubertal development (presenting at the age of 14 to 15 years with pubic hair and breast development at Tanner stage II) and high gonadotropin levels as well as LH levels ranging from 38 to 60 IU/l and FSH levels of between 50 and 92 IU/l. Imaging studies (by both ultrasound and MRI) could not detect ovarian tissue, and a small uterus was consistently observed in all affected individuals. Other female siblings of the affected females (IV-2, IV-3, and IV-4, Figure 1A), currently aged 20 to 50 years, are healthy, with normal pubertal development, menstrual cycles, and fertility. The mothers of the affected women had menarche at a normal age. All 5 affected women are otherwise healthy and have no other developmental or neurological deficits. All the men in the family had normal pubertal development, gaining secondary sexual characteristics, and the married men have multiple children. Thus, there is currently no evidence for defects in male sexual development or male infertility in this family. Given the pedigree structure and consanguinity, the most probable mode of inheritance of the XX-GD in this family is autosomal recessive.

Genetic analysis

Homozygosity mapping was performed using SNP arrays in affected females IV-1, IV-5, IV-6, and IV-7 and in the healthy female IV-2 (Figure 1A) to detect informative genomic regions that were homozygous and shared among affected individuals but not an unaffected sibling. This analysis identified two large regions spanning a total of 9.3 Mb that fulfilled homozygosity criteria on chromosomes 4 (chr4:152,221,451-157,617,198, hg19) and 12 (chr12:68,756,371-72,742,353, hg19). None of the genes in these homozygous regions had known functions that would indicate them as clear candidates for XX-GD. Whole-exome sequencing was performed in two affected cousins (IV-1 and IV-5, Figure 1A). Candidate variants that were absent in databases and predicted as damaging and homozygous in both affected individuals were further filtered for cosegregation using the SNP genotyping data (see Methods and Supplemental Table 1; supplemental material available online with this article; doi:10.1172/JCI83553DS1). Only a single variant in the *NUP107* gene at chr12:69,115,648 (c.1339G>A, p.D447N) fulfilled all filtering criteria. Sanger sequencing of this variant in all sampled individuals (Figure 1B) showed that *NUP107*, c.1339G>A, was homozygous in all affected females, segregated as expected in the family (consistent with autosomal recessive inheritance, Figure 1, A and B), and was not present in 150 ethnically matched healthy controls. The aspartic acid residue altered by the p.D447N mutation is highly conserved across species, including in the *Drosophila melanogaster Nup107* gene (corresponding to D364), and resides within a highly conserved stretch of amino acids (Figure 1C).

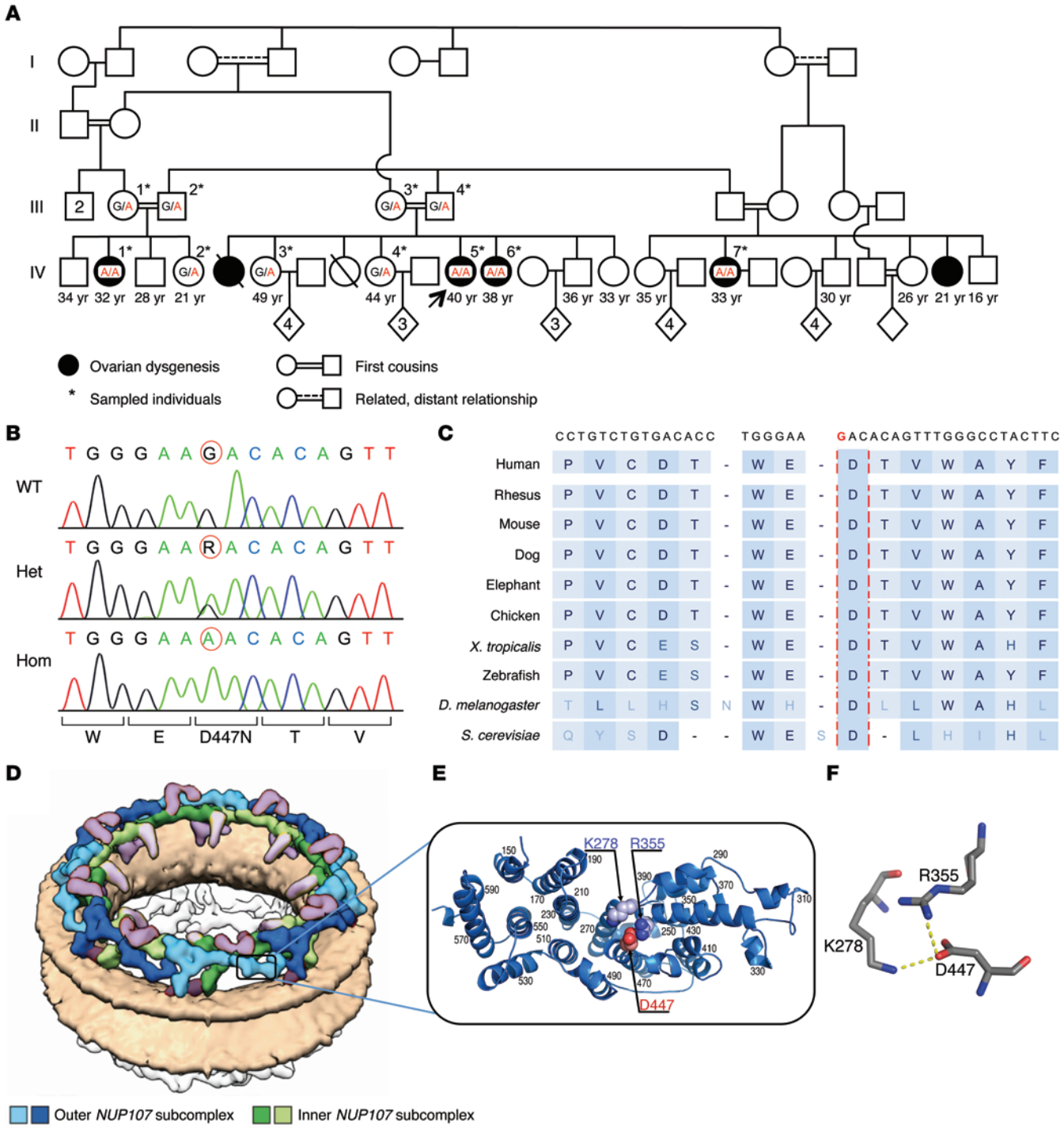

Figure 1. An extended consanguineous family with XX-GD. (**A**) Family pedigree. The proband is indicated by an arrow. Pedigree numbers of individuals are indicated above the symbols and ages are indicated beneath. The *NUP107* c.1339G>A (p.D447N) WT (G) and the variant (A) nucleotides are indicated. (**B**) Sanger sequencing of the *NUP107* c.1339G>A variant in genomic DNA of WT, heterozygous, and homozygous individuals. Nucleotides are indicated above the sequences, and amino acid residues are marked below; the c.1339G>A variant position is circled in red. (**C**) Evolutionary conservation of the NUP107 residue D447. The nucleotide sequence flanking c.1339 is indicated above, with the mutated nucleotide in red, and corresponding residues in various species are shown below. The region including D447 is highly conserved, and D447 (highlighted by vertical red lines) is conserved in all species shown, including in *Drosophila melanogaster*, as well as in all other *Drosophila* species (data not shown). (**D** and **E**) Structural modeling of the NUP107 p.D447N mutation. (**D**) Illustration of the 3D arrangement of the human *NUP107* complex within the NPC scaffold on the nuclear membrane (colored peach). All 16 copies of the human *NUP107* subcomplex within the cytoplasmic ring are shown. The inner and outer subcomplexes are colored green and blue, respectively, and adjacent nucleoporins and subcomplexes are colored purple (adapted from ref. 24). (**E**) Model of the NUP107 NTD, with D447 colored red and K278 and R355 colored purple. This figure was prepared using PyMol (71). (**F**) D447 forms salt bridges with K278 and R355. The salt bridges between D447 and K278 and R355 are indicated by broken yellow lines. The N447 mutant changes the overall charge of NUP107 and abolishes these salt bridges. This figure was prepared using PyMol (71).

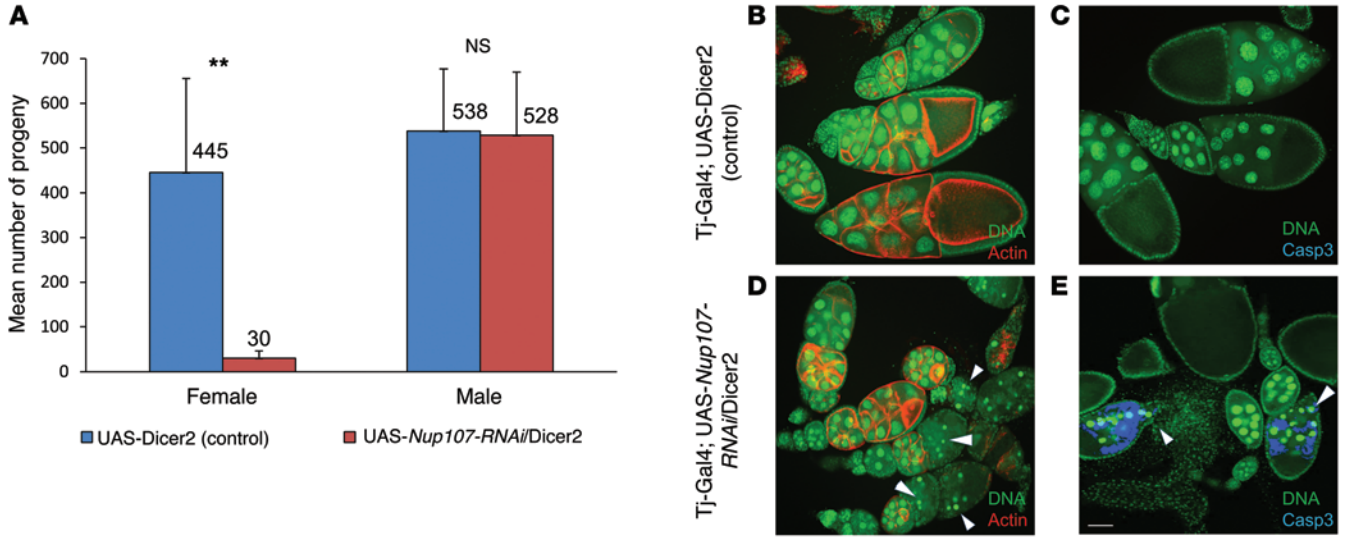

Figure 2. Gonadal somatic cell knockdown of *Nup107* in *Drosophila*. (**A**) Reduced total number of progeny in female *Nup107-RNAi* knockdown flies. Mean number of progeny in UAS-*Nup107-RNAi*/UAS-dicer2 flies compared with that in control UAS-Dicer2 female or male flies, expressed with the gonadal somatic–specific Tj-Gal4 driver. *Nup107* knockdown in female flies results in 15-fold fewer progeny. *Nup107* knockdown in male flies does not affect the number of progeny. The mean number of progeny in >10 flies in each of 4 independent experiments is indicated above the bars. $^{**}P = 0.007$, 2-tailed, unpaired Student's *t* test. (**B**–**E**) Structural defects and apoptosis in ovarioles of *Nup107-RNAi* knockdown and control flies. (**B** and **C**) Tj-Gal4; UAS-dicer2 control ovarioles. Control egg chambers. DNA in the nurse cells appears normal (green), (**B**) overall egg chamber structure is intact (normal actin staining [red]), and (**C**) no apoptosis is observed (no caspase-3 staining [blue]). (**D** and **E**) Tj-Gal4; UAS-*Nup107-RNAi*/UAS-dicer2 ovarioles. Egg chambers in *Nup107-RNAi* knockdown flies, expressed using the somatic gonadal-specific tj-Gal4 driver. (**D** and **E**) DNA in the nurse cells appears condensed and punctate (arrowheads). (**D**) Disintegration of the egg chamber structure is observed around these condensed nuclei (no actin staining), and (**E**) apoptosis is apparent (caspase-3 staining). DNA was stained by Sytox (green), actin was stained by rhodamine phalloidin (red), and apoptosis was identified using anti-cleaved caspase-3 (casp-3) staining (blue). Scale bar: 100 μm.

Analysis of protein structure

Nucleoporins and their subcomplexes assemble to form the scaffold of the NPC (Figure 1D and ref. 24). The human nucleoporin protein NUP107 (UniProt ID P57740) consists of two domains: the N-terminal domain (NTD) corresponding to residues 1–600 and the C-terminal domain (CTD) comprising residues 601–925. While the structure of the CTD is available (Protein Data Bank [PDB] ID 3CQC, ref. 25; and PDB ID 3I4R, ref. 26), the structure of the NTD containing the D447N mutation is not. A homology model constructed for this domain based on the yeast ortholog *Nup84* (PDB ID 3IKO) shows that the NTD adopts a fully α-helical secondary structure (Figure 1E), in which the negatively charged D447 is partially exposed and forms salt bridges with positively charged K278 and R355 (Figure 1F). The D447N mutation changes the negative charge into a neutral one, which abolishes these salt bridges, predicting a destabilization of the overall NUP107 protein fold in this region and possible impairment of *NUP107*'s interaction with other subunits in the NPC. Specifically, *NUP107* is the critical anchor to the NPC for *NUP133*, positioning *NUP133* at the NPC periphery (25), and the D447N mutation is likely to compromise the tight compact interface tail-to-tail interaction between the CTD of *NUP107* (amino acids 658–925) and the CTD of the nucleoporin *NUP133* (amino acids 935–1,156) (PDB ID 3CQC).

Drosophila melanogaster model

Gonadal knockdown of Nup107 results in female-specific sterility. Whereas the XX-GD phenotype is specific and tissue restricted, *NUP107* is ubiquitously expressed, and the NPC is present in every nucleated cell. Therefore, before modeling the specific missense mutation identified in family A, we first performed gonadal knockdown of *Nup107* in *Drosophila* to determine whether *Nup107* functions in the ovary. We chose *Drosophila* as a model, because *Drosophila* nucleoporins, including *Seh1* and *Nup154*, were shown to play a role in oogenesis (27, 28), and there is high degree of amino acid conservation between human and *Drosophila* Nup107 proteins (35% identity and 54% similarity, with 5% gaps). *Nup107* expression was knocked down using a UAS-*Nup107-RNAi* line in combination with the traffic jam–Gal4 (tj-Gal4) driver line, which is expressed in gonadal somatic cells of both sexes throughout development (29). In male flies, gonadal *Nup107* knockdown had no apparent effects, including a lack of effect on viability or fertility (Figure 2A). In female flies, gonadal *Nup107* knockdown resulted in universal infertility; these females laid 15-fold fewer eggs (Figure 2A, $P = 0.007$). Analysis of ovarioles from these infertile females revealed extensive disintegration of their egg chambers compared with those of controls, including condensation of DNA in the nurse cells, accompanied by cell death (Figure 2, B–E).

Reduced fertility in the female Nup107^{D364N} Drosophila transgenic model. To model the human NUP107 p.D447N mutation in *Drosophila*, we used the recently described null allele of the *Drosophila Nup107* gene (*Nup107^{E8}*) in conjunction with a transgenic rescue construct (30). The null allele, which lacks 976 bp of the open reading frame, including the start ATG codon, was generated using P element imprecise excision (30), and homozygosity for this *Nup107^{E8}* allele is lethal. An RFP-*Nup107* genomic rescue transgene containing the *Nup107* gene (including 5′ and 3′ regulatory regions)

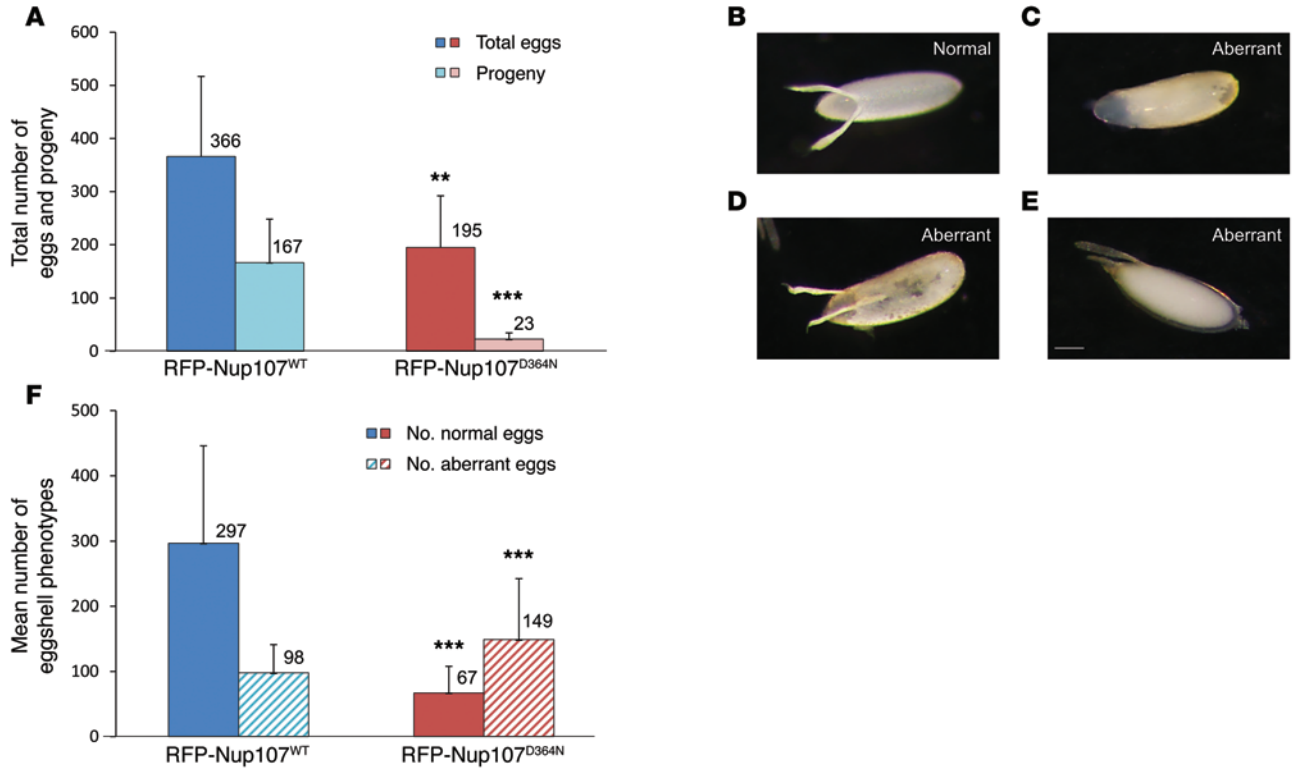

Figure 3. Impaired fertility and eggshell morphology in RFP-Nup107^{D364N} mutant transgenic rescued flies. (**A**) The total number of eggs and progeny is reduced in RFP-Nup107^{D364N} mutant transgenic rescued flies. The total number of laid eggs in transgenic rescued females is reduced by 47% in RFP-Nup107^{D364N} mutant flies compared with that in RFP-Nup107^{WT} flies (**P = 0.01). The number of progeny from transgenic rescued females is 7.2 times lower in RFP-Nup107^{D364N} mutant flies compared with that in RFP-Nup107^{WT} flies (***P = 0.0001). Hatch rate (progeny per total eggs) is only 12% in RFP-Nup107^{D364N} mutant females compared with 45% in RFP-Nup107^{WT} transgenic rescued females (P = 2.6E^{-7}). The numbers of progeny or eggs are indicated above the bars. Results shown are the mean of >3 experiments, with >10 flies each. (**B**–**E**) Eggshell phenotypes. (**B**) Normal eggshell phenotype. (**C**–**E**) Representative images of aberrant eggshell phenotypes, including dorsal appendage and chorion defects: (**C**) lack of dorsal appendages, (**D**) misshapen dorsal appendages, and (**E**) aberrantly located dorsal appendages. Aberrant chorions appear far more translucent than the normally opaque chorion. Scale bar: 100 μm. (**F**) Quantification of aberrant eggshell phenotypes in RFP-Nup107^{D364N} mutant transgenic rescued flies. In transgenic rescued female flies, the proportion of eggs with aberrant eggshell phenotypes was 69% (149 of 216) in RFP-Nup107^{D364N} mutants compared with 25% (98 of 395) in RFP-Nup107^{WT} flies (***P = 3.5E^{-14}). The numbers of aberrant eggshell phenotypes are indicated above the bars. Results shown are the mean of >3 experiments, including >10 flies each. Statistical significance was assessed by a 2-tailed, unpaired Student's t test.

fused to RFP has been shown to rescue the lethal phenotype of the *Nup107^{E8}* deletion allele (w; *Nup107^{E8}/Nup107^{E8}*; P[w+, RFP-*Nup107*] flies), demonstrating both that *Nup107* is an essential gene and that the tagged rescue transgene is functional (30).

Based on this system, we generated two versions of RFP-*Nup107* transgenic rescued flies, one containing the WT gene (RFP-Nup107^{WT}) and the other containing a missense mutation p.D364N (RFP-Nup107^{D364N}), which corresponds to the identified human missense mutation, p.D447N (Figure 1, B and C). Several independent transgenic fly stocks were generated, expressing either the WT or the mutant RFP-Nup107 protein. Notably, in all transgenic fly stocks, both RFP-Nup107^{WT} and mutant RFP-Nup107^{D364N} proteins were correctly localized to the nuclear envelope, indicating that the mutation does not affect normal protein localization (Supplemental Figure 1).

For further characterization, we chose third chromosome WT and mutant RFP-*Nup107* insertion stocks that were viable as homozygotes and expressed the transgene at similar levels (as determined by quantitative real-time PCR, Supplemental Figure 2). We found that, in RFP-Nup107^{WT} and in the RFP-Nup107^{D364N} mutant transgenic lines, the transgenes rescued the lethality of the homozygous *Nup107^{E8}* deletion allele (yw; *Nup107^{E8}/Nup107^{E8}*; RFP-Nup107^{WT} or RFP-Nup107^{D364N}). Importantly, no overt morphological defects were apparent in either RFP-Nup107^{WT} or RFP-Nup107^{D364N} mutant rescued flies, indicating that neither the RFP tag nor the D364N mutation interfere with general development.

We then assessed the effect of the Nup107 p.D364N mutation on fertility in female flies. We found that RFP-Nup107^{D364N} mutant rescued females had significantly reduced fertility compared with that of RFP-Nup107^{WT} rescued females. Nup107^{D364N} mutant transgenic rescued females had 7.2-fold fewer progeny than RFP-Nup107^{WT} transgenic rescued females (Figure 3A, P = 0.0001). Further analysis showed that mutant transgenic rescued females laid 47% fewer eggs compared with WT transgenic rescued females (Figure 3A, P = 0.01) and that hatch rates in Nup107^{D364N} mutant transgenic rescued females were 4-fold lower than those in WT transgenic rescued females (Figure 3A, P = 2.6E^{-7}). These results demonstrate that oogenesis is perturbed by the D364N mutation. Those eggs that do hatch are able to develop and produce viable adult flies, with no apparent morphological defects.

Closer analysis of the laid eggs revealed abnormal eggshell phenotypes, including a range of chorion and dorsal appendage defects

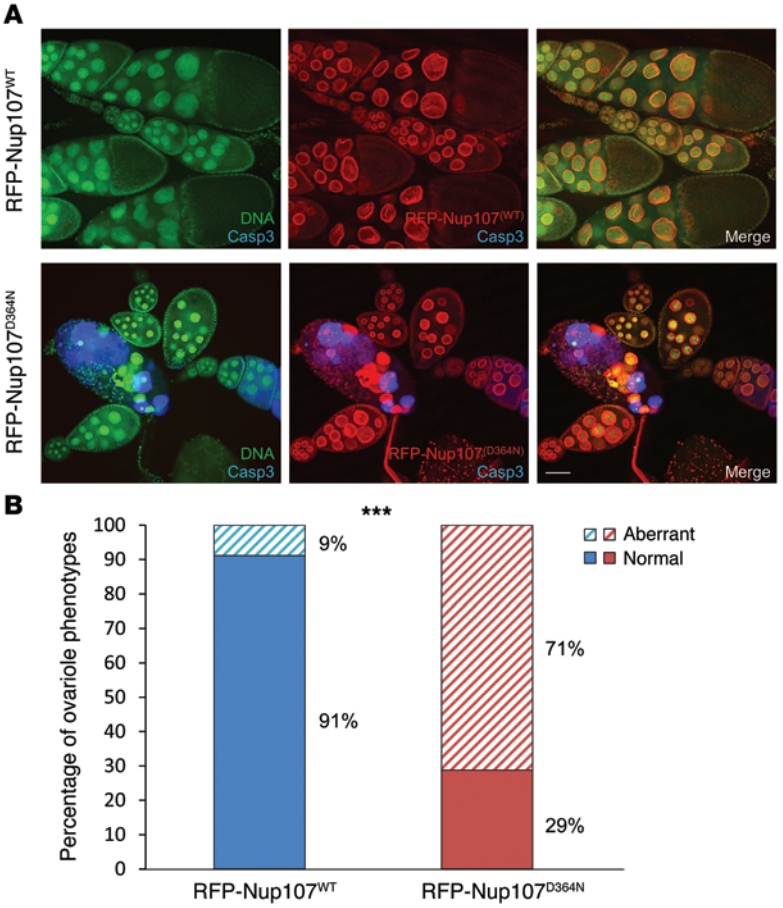

Figure 4. Ovariole disintegration and apoptosis in RFP-Nup107^{D364N} mutant transgenic rescued female flies. (**A**) Representative images of RFP-Nup107^{D364N} and RFP-Nup107^{WT} ovarioles. In ovarioles of an RFP-Nup107^{WT} fly, DNA in the developing egg chambers appears normal (green), the nuclear envelope is intact (red) and encircling the nuclear DNA, and no cleaved caspase-3 staining is observed, indicating no apparent apoptosis. In ovarioles of an RFP-Nup107^{D364N} mutant fly, nuclear DNA (green) in many nurse cells appears condensed and punctate, with disintegration of the nuclear envelope structure (red) adjacent to the condensed nuclei. Cleaved caspase-3 (blue) is highly expressed in the collapsed nurse cells, indicating extensive apoptosis in these cells. DNA staining was performed with Sytox (green), RFP-Nup107^{WT} or RFP-Nup107^{D364N} nuclear envelope staining was performed with RFP (red), and staining for apoptosis was performed with anti-cleaved caspase-3 (blue). Ovarioles were assessed at stage 9 to 10. Scale bar: 100 μm. (**B**) Quantification of disintegrating ovarioles in RFP-Nup107^{D364N} and RFP-Nup107^{WT} ovaries. General ovariole disintegration (as indicated by punctate nurse cell DNA and positive cleaved caspase-3 staining, as shown in **A**) was observed in 71% and only 9% of ovarioles in RFP-Nup107^{D364N} mutant and Nup107^{WT} transgenic rescued females, respectively. For each phenotype, data shown are for n = 90 ovarioles from Nup107^{WT} ovaries and n = 125 ovarioles from Nup107^{D364N} ovaries from 2 experiments, each from 15 flies. ***P = 0.001, 2-tailed, unpaired Student's t test.

(Figure 3, C–E). Aberrant eggshell phenotypes were observed in 69% of the eggs laid by mutant transgenic rescued females compared with only 25% of the eggs laid by WT transgenic rescued females (Figure 3F, $P = 3.5E^{-14}$). The aberrant chorions appeared far more translucent than the normal opaque chorion (Figure 3B), which is indicative of a thin eggshell. Abnormal eggs were more fragile, and many appeared collapsed. The aberrant dorsal appendages appeared shorter or thicker than normal, and some eggs had flaccid dorsal appendages that were fused along the base.

Finally, dissection of the ovaries of these infertile RFP-Nup107^{D364N} mutant transgenic rescued females revealed striking morphological defects, including general ovariole disintegration (Figure 4A). In 71% of D364N mutant ovarioles, the nuclear envelope of nurse cells, marked by the mutant RFP-Nup107^{D364N} protein, collapsed to a punctate feature and no longer contained the nuclear DNA, which appeared fragmented and condensed (Figure 4). Caspase-3 staining demonstrated extensive apoptosis in the disintegrating egg chambers (Figure 4A). In sharp contrast, these aberrant features were observed in only 9% of ovarioles from RFP-Nup107^{WT} transgenic rescued females (Figure 4B, $P = 0.001$).

Discussion

We report a recessive missense mutation in *NUP107* (c.1339G>A, p.D447N) as a genetic basis for human XX-GD. This mutation alters a highly conserved aspartic acid residue and is predicted to disrupt salt bridges in the NTD of the NUP107 protein (Figure 1, D–F). Gonadal *Nup107* RNAi knockdown in *Drosophila*, using the tj-Gal4 driver, resulted in female-specific infertility (Figure 2A). Although the tj-Gal4 driver is expressed only in a subpopulation of the gonadal somatic cells (escort cells, follicular stem cells, and follicle cells) (31–33), we observed defects also in the nurse cells and in the oocytes (Figure 2, D and E). This non-cell-autonomous effect may suggest that Nup107 acts by influencing the activity and/or transport of signals/factors in the gonadal somatic cells that are important for the correct differentiation of nurse cells and oocytes. Modeling the corresponding D364N mutation in *Drosophila* female flies led to reduced fertility and defective oogenesis. Compared with RFP-Nup107^{WT}, RFP-Nup107^{D364N} transgenic females had 7.2 times fewer progeny ($P = 0.0001$), reflecting a 47% reduction in the number of eggs laid ($P = 0.01$) and a 4-fold reduction in the proportion of hatched eggs ($P = 2.6E^{-7}$) (Figure 3A). In RFP-Nup107^{D364N} and RFP-Nup107^{WT} transgenic mutated females, respectively, defective eggshells were observed in 69% versus 25% of eggs (Figure 3, C–F, $P = 3.5E^{-14}$), and ovariole disintegration, nurse cell nuclear envelope collapse, and extensive egg chamber cell death were found in 71% versus 9% of ovarioles (Figure 4, $P = 0.001$). No general morphological defects were observed in Nup107 p.D364N homozygous transgenic flies, whereas the background *Nup107^{E8}* deletion allele was lethal. Normal general development, together with the profound specific effect of the D364N mutation on *Drosophila* oogenesis, provides further evidence that the human NUP107 p.D447N mutation underlies XX-GD, thus demonstrating for the first time to our knowledge a critical role for *NUP107* in ovarian function.

The NUP107 protein belongs to the nucleoporin family and is an essential component of the ubiquitous NPC. The NPC is a multisubunit protein structure embedded into the nuclear envelope, which enables active and passive transport between the cytoplasm and the nucleus. The selective access of regulatory factors to the nucleus and export of specific RNA molecules mediated by the NPC are mandatory for cell-specific gene expression and signal transduction (34, 35). NUP107 is the main component in the NUP107-160 complex, which includes 9 nucleoporin components, forming the outer ring of the NPC scaffold (Figure 1D and ref. 36). Accumulating evidence indicates that NPC components have roles beyond their function as the nucleus-cytoplasm conduit and may affect chromatin regulation and nuclear trafficking (37, 38). The "gene gating" hypothesis proposes that nuclear pores specifically interact with active genes to promote coregulation of transcription with mRNA export (39). Such links between nucleoporins and active genes have been demonstrated in multicellular organisms; analysis of the chromatin-binding behavior of *Drosophila* nucleoporins revealed the presence of several NPC components at active genes (38, 40). The "gene looping" model (41) proposes that NPC components are associated with boundaries of different chromatin domains and insulate euchromatic regions from the silencing environment of adjacent heterochromatin. Indeed, several components that tether euchromatin-heterochromatin boundary elements to the NPCs have been found to protect euchromatic regions from silencing (42). Such roles in regulation of gene expression may explain why the NPC, although present in every nucleated cell, has been shown to have multiple tissue-specific roles (43). Indeed, the two previous known human diseases caused by germline mutations in nucleoporin genes are organ limited: *NUP155* mutations cause familial atrial fibrillation (MIM #615770) (44), and a *NUP62* mutation results in infantile striatonigral degeneration (MIM #271930) (45).

Several nucleoporins have been implicated in fertility. SEH1 is a conserved component of the NUP107-160 complex. In *Drosophila,* SEH1 associates with MIO, a protein required for maintenance of the meiotic cycle and oocyte fate during oogenesis (28), and *Seh1* mutant *Drosophila* females show altered mitotic progression of germ cells, failure to maintain the meiotic cycle, and defective oocyte differentiation. NUP154 is also an essential nucleoporin conserved across species from yeast to humans. Studies on hypomorphic mutant alleles of *Nup154* in *Drosophila* demonstrated that Nup154 in males is required for testicular cyst formation, control of spermatocyte proliferation, and meiotic progression (27). In *Drosophila* females, Nup154 is essential for egg chamber development and oocyte growth (27, 46, 47). Interestingly, in mutant egg chambers, the Nup154 protein accumulated in the cytoplasm, while it was only barely detected at its usual functional location in the nuclear envelope. Aladin, a protein localized to the NPC, is a third NPC element that has been shown to be associated with ovarian dysfunction. As in mice, *Aladin* KO females are sterile despite apparently normal ovarian histology, follicular development, and ovulation (48). However, it is possible that Aladin exhibits a yet unknown effect on the meiosis and oocyte maturation, and interestingly, in humans, *ALADIN* mutations result in a different phenotype, Achalasia-Addisonianism-Alacrima syndrome (MIM #231550). We did not observe mislocalization of mutant Nup107 (Supplemental Figure 1), as observed for mutant Nup154. Gonadal-specific effects could be exerted in several ways. NUP107 might regulate expression of gonadal-specific gene(s) by either chromatin regulation or protein nuclear trafficking. NUP107 may also interact with tissue-specific factors required for development/maintenance of the gonad, as in the case of the SEH1-MIO interaction. Further research is required to identify whether the function of any gonadal-specific proteins is impaired as a result of the NUP107 mutation. Modeling this in RFP-Nup107^{D364N} mutant *Drosophila* ovaries is now feasible.

A major cellular function that is both associated with normal NPC activity and implicated in XX-GD is the DNA damage response, which is required to repair double-strand breaks induced by homologous recombination in meiosis I (49). In oocytes, a DNA damage checkpoint is activated at the time of meiotic arrest (50), and as noted above, XX-GD can result from mutations in the *MCM8* (8, 9) and *MCM9* (7) genes, which are required for double-strand break repair. A series of nucleoporin mutants in yeast and metazoan cells show accumulation of DNA damage and hypersensitivity to DNA-damaging agents (51–53), and downregulation of several subunits of the NUP107-160 complex generates spontaneous DNA damage in human cells (54). A very recent report indicates that, in response to DNA damage, the apoptotic protease-activating factor 1 (Apaf-1), which mediates cell-cycle arrest in response to genotoxic stress, is translocated to the nucleus via direct binding to Nup107 (55). This raises the possibility that *Nup107* mutations compromise the meiotic DNA damage response, leading to oocyte death. Such a role for Nup107 would be consistent with the general disintegration and apoptosis observed in the ovarioles of the *Drosophila* RFP-Nup107^{D364N} mutant transgenic females we describe. Further studies will be necessary to determine whether ovary-specific proteins interact with Nup107 and whether it indeed plays a role in homologous recombination repair.

In conclusion, we report a genetic basis for XX-GD and a human mutation, p.D447N in the *NUP107* gene, that we believe to be novel, demonstrating a pivotal role for NUP107 in ovarian function. *Nup107* knockdown in *Drosophila* ovarian somatic cells caused female-specific sterility and the corresponding missense mutation in the *Drosophila* Nup107 protein, p.D364N, mimicked the human phenotype of female sterility and ovarian abnormalities. These findings implicate what we believe to be a novel pathway in the normal development and/or maintenance of the ovary and expand our knowledge of the networks that may also be involved in milder phenotypes, such as premature ovarian failure.

Methods

DNA extraction. Genomic DNA was extracted from peripheral blood mononuclear cells as previously described (56, 57).

Microarray analysis. Genomic DNA was genotyped with the Affymetrix Gene Chip 250 K/750 K Nsp SNP array. The data have been deposited in NCBI's Gene Expression Omnibus (accession GSE72159) (58). SNP data were analyzed using KinSNP (59) to detect informative genomic regions that were homozygous and shared among affected individuals but not their unaffected siblings. In individuals in whom whole-exome analysis was not performed, SNP genotypes were used to predict segregation of candidate variants identified in

exomed individuals. This was done by comparing SNP genotypes at the genomic location surrounding each variant. In nonexomed individuals, a variant was considered to cosegregate with the phenotype if the surrounding SNPs were homozygous for the same allele in all affected persons and were heterozygous or homozygous for the other allele in the unaffected person.

Whole-exome, massively parallel sequencing. Libraries prepared from genomic DNA were hybridized to biotinylated cRNA oligonucleotide baits from the SureSelect Human All Exon Kit (Agilent Technologies). Each exome-enriched library was sequenced with 50-bp paired-end reads on two lanes of an ABI SOLiD-3 plus analyzer. Raw data have been deposited in NCBI's Sequence Read Archive (accession SRP062710) (60). The sequences were aligned to the hg19 human genome assembly (February 2009) using BWA (61). Samtools (62) was used to list high quality DNA variants. The variants were then classified by Annovar (63) as missense, nonsense, frameshift, or splice-site variants. Variants were filtered by a frequency of ≤1% in dbSNP (64) or in the Exome Variant Server (65); by probability to damage the protein's structure or function, according to the prediction tools polyphen2 (66) and SIFT (67) (polyphen2 ≥0.6, SIFT ≤0.05); and by homozygous genotype and whether this genotype is shared between both affected cousins and present in the previously identified homozygous regions. Detailed filtering data are shown in Supplemental Table 1.

Sanger sequencing for the NUP107 c.1339G>A mutation. Primers flanking the *NUP107* (c.1339G>A, p.D447N) mutation were used for PCR amplification: (5′→3′) forward TCATTGGATGTAATTGCTTTTCC and reverse TCAAAACAATCCAACAAACTCA. The 245-bp PCR products were sequenced using BigDye Terminator v1.1 and analyzed on a 3130xl Genetic Analyzer (Applied Biosystems).

Restriction assay in controls for the NUP107 mutation. The *NUP107* c.1339G>A mutation abolishes a *Bbs*I restriction site. Primers flanking the *NUP107* c.1339G>A mutation were used to amplify genomic DNA of 150 ethnically matched controls: (5′→3′) forward TCATTGGATGTAATTGCTTTTCC and reverse TCAAAACAATCCAACAAACTCA. The 245-bp PCR products were digested with *Bbs*I (New England Biolabs) and run on 3% agarose gels.

Structural modeling of human NUP107. Sequences of Nup84 and NUP107 proteins were aligned using MAFFT (68) and manually rectified to maintain secondary structure elements as predicted by PSIPRED (69). To build the 3D model of the human NUP107 NTD (residues 114–600), the crystal structure of yeast Nup84 (PDB ID 3IKO, chain F, residues 7–442) was used as a template. The sequence alignment of model templates was extracted from the multiple sequence alignment and was used to construct the model using Modeller 9.9 (70). To generate the mutant structure of NUP107 p.D447N, the residue was mutated using the PyMol mutagenesis tool (71).

Fly strains. The following stocks were used in this study: w; tj-Gal4; UAS-dicer-2 (a gift from Lilach Gilboa, Weizmann Institute of Science, Rehovot, Israel), *Nup107*^{E8} (Bloomington Drosophila Stock Center, Department of Biology, Indiana University, catalog 35516), and UAS-*Nup107-RNAi* (Vienna *Drosophila* RNAi Center, 22407 and 110759).

Drosophila Nup107-RNAi knockdown. In both male and female flies, *Nup107* was knocked down using a UAS-*Nup107-RNAi* line in combination with the tj-Gal4 driver line, which is expressed in gonadal somatic cells of both sexes (w; tj-Gal4; UAS-dicer-2/UAS-*Nup107-RNAi*).

Immunostaining and imaging. Fixation and immunostaining of gonads were performed in accordance with standard protocols. Rabbit polyclonal anti-cleaved caspase-3 antibody was used at a dilution of 1:100 (Asp175, 9661, Cell Signaling Technology). Cy5-conjugated secondary antibody (donkey anti-IgG antibody, 711-175-152, Jackson Immunoresearch Laboratories) was used at 1:100 dilutions. For DNA staining, Sytox Green stain (S7020, Molecular Probes) was used at a concentration of 1:1,000. Actin visualization was performed by rhodamine phalloidin staining (R415, Molecular Probes) at a concentration of 1:250. Images were taken on a TE2000-E confocal microscope (Nikon) using ×10 or ×20 objectives. Figures were edited using Adobe Photoshop 7.0.

Mutagenesis and generation of RFP-Nup107^{WT} *or RFP-Nup107*^{D364N} *mutant transgenic flies*. A pCasper expression construct containing the *Drosophila Nup107* genomic sequence (spanning 1.5 kb upstream and 0.8 kb downstream of *Nup107* ORF) was provided by Valérie Doye (Cell Biology Program, Institut Jacques Monod, UMR 7592 Centre National de la Recherche Scientifique–Université Paris Diderot, Paris, France) (30). Site-directed mutagenesis was performed to create the Nup107 p.D364N mutation (corresponding to the human NUP107 p.D447N mutation) using the QuikChange Lightning Site-Directed Mutagenesis Kit (Agilent Technologies) according to the manufacturer's instructions, with the following primers: forward CACAGCAACTGGCACAATTTGCTCTGGGCCC and reverse GGGCCCAGAGCAAATTGTGCCAGTTGCTGTG. 50 μg of purified DNA was injected into mutant embryos lacking the gene W (for red eyes, BestGene Inc.). Adult flies were single crossed to yw, and F_1-containing red eyes were selected. Transgenic flies were kept as balanced stocks. Transgenic stocks with the rescuing P element integrated into the third chromosome were crossed into the *Nup107*^{E8}-null background.

Quantitative real-time PCR analysis. Ten ovaries were collected from each yw; *Nup107*^{E8}/*Nup107*^{E8};RFP-Nup107^{WT}, yw; *Nup107*^{E8}/*Nup107*^{E8};RFP-Nup107^{D364N}, and control yw adult female flies. Tissues were disrupted using TRI Reagent (Sigma-Aldrich). RNA was reverse transcribed using random hexamers in the presence of RNase inhibitor (rRNasin, Promega). Quantitative RT-PCR reactions were performed using a TaqMan assay for the *Drosophila Nup107* gene (Applied Biosystems, assay ID: Dm01810501_g1) on an ABI PRISM 7900 (Applied Biosystems). Ct values were normalized to the Ct values of the *Drosophila* housekeeping gene *RpS17* (Applied Biosystems, assay ID: Dm01822503_g1) in each relevant sample. Relative mRNA levels were quantified using the comparative method (ABI PRISM 7700 Sequence Detection System, Thermo Fisher Scientific Inc.) and calculated as $2^{-\Delta Ct}$. Experiments were performed with 4 independent replications, each time with triplicate wells for each sample.

Statistics. Statistical significance was assessed by a 2-tailed, unpaired Student's *t* test. *P* values of less than 0.05 were considered significant. Data are shown as mean ± SEM.

Study approval. The study was approved by the IRB of Shaare Zedek Medical Center (approval no. 20/10) as well as the Israel National Ethics Committee for Genetic Studies. Informed consent was obtained from all participants or their legal guardians.

Acknowledgments

This study was supported by the US Agency for International Development program for Middle East Regional Cooperation

(grant TA-MOU-10-M30-021 to E. Levy-Lahad and M. Kanaan), by a generous gift from the Hassenfeld family (to Shaare Zedek Medical Center), by the Israel Science Foundation (grant 960/13 to O. Gerlitz), and by the Legacy Heritage Biomedical Program of the Israel Science Foundation (grant 1531/09 to D. Zangen and grant 1788/15 to O. Gerlitz and D. Zangen). We thank V. Doye, L. Gilboa, the Vienna *Drosophila* RNAi Center, and the Bloomington *Drosophila* Stock Center for reagents and fly stocks. We thank U. Abdu for advice on the *Drosophila* oogenesis studies. We also thank Mira Korner, Michal Bronstein, and Temima Schnitzer-Perlman at the Center for Genomic Technologies at the Hebrew University of Jerusalem for performing genomic sequencing using the SOLiD platform.

Address correspondence to: David Zangen, Division of Pediatric Endocrinology and Diabetes, Hadassah Hebrew University Medical Center, Jerusalem 91240, Israel. Phone: 972.2584.4430; E-mail: zangend@hadassah.org.il. Or to: Offer Gerlitz, Developmental Biology and Cancer Research, Institute for Medical Research Israel-Canada, Hebrew University, Faculty of Medicine, Jerusalem 91120, Israel. Phone: 972.2675.7528; E-mail: offerg@ekmd.huji.ac.il. Or to: Ephrat Levy-Lahad, Medical Genetics Institute, Shaare Zedek Medical Center, Shmu'el Bait St 12, Jerusalem 91031, Israel. Phone: 972.2666.6136; E-mail: lahad@szmc.org.il.

Ziva Ben-Neriah's present address is: Medical Genetics Institute, Shaare Zedek Medical Center, Jerusalem, Israel.

1. Hughes IA. Disorders of sex development: a new definition and classification. *Best Pract Res Clin Endocrinol Metab*. 2008;22(1):119–134.
2. Vainio S, Heikkila M, Kispert A, Chin N, McMahon AP. Female development in mammals is regulated by Wnt-4 signalling. *Nature*. 1999;397(6718):405–409.
3. Biason-Lauber A, Konrad D, Navratil F, Schoenle EJ. A WNT4 mutation associated with Mullerian-duct regression and virilization in a 46,XX woman. *N Engl J Med*. 2004;351(8):792–798.
4. Kamata T, Katsube K, Michikawa M, Yamada M, Takada S, Mizusawa H. R-spondin, a novel gene with thrombospondin type 1 domain, was expressed in the dorsal neural tube and affected in Wnts mutants. *Biochim Biophys Acta*. 2004;1676(1):51–62.
5. Radi O, et al. XX sex reversal, palmoplantar keratoderma, and predisposition to squamous cell carcinoma: genetic analysis in one family. *Am J Med Genet A*. 2005;138A(3):241–246.
6. Zangen D, et al. XX ovarian dysgenesis is caused by a PSMC3IP/HOP2 mutation that abolishes coactivation of estrogen-driven transcription. *Am J Hum Genet*. 2011;89(4):572–579.
7. Wood-Trageser MA, et al. MCM9 mutations are associated with ovarian failure, short stature, and chromosomal instability. *Am J Hum Genet*. 2014;95(6):754–762.
8. AlAsiri S, et al. Exome sequencing reveals MCM8 mutation underlies ovarian failure and chromosomal instability. *J Clin Invest*. 2015;125(1):258–262.
9. Tenenbaum-Rakover Y, et al. Minichromosome maintenance complex component 8 (MCM8) gene mutations result in primary gonadal failure. *J Med Genet*. 2015;52(6):391–399.
10. Le Quesne Stabej P, et al. STAG3 truncating variant as the cause of primary ovarian insufficiency [published online ahead of print June 10, 2015]. *Eur J Hum Genet*. doi:10.1038/ejhg.2015.107.
11. de Vries L, Behar DM, Smirin-Yosef P, Lagovsky I, Tzur S, Basel-Vanagaite L. Exome sequencing reveals SYCE1 mutation associated with autosomal recessive primary ovarian insufficiency. *J Clin Endocrinol Metab*. 2014;99(10):E2129–E2132.
12. Di Pasquale E, Beck-Peccoz P, Persani L. Hypergonadotropic ovarian failure associated with an inherited mutation of human bone morphogenetic protein-15 (BMP15) gene. *Am J Hum Genet*. 2004;75(1):106–111.
13. Dixit H, et al. Missense mutations in the BMP15 gene are associated with ovarian failure. *Hum Genet*. 2006;119(4):408–415.
14. Park SY, Jameson JL. Minireview: transcriptional regulation of gonadal development and differentiation. *Endocrinology*. 2005;146(3):1035–1042.
15. Edson MA, Nagaraja AK, Matzuk MM. The mammalian ovary from genesis to revelation. *Endocr Rev*. 2009;30(6):624–712.
16. Persani L, Rossetti R, Di Pasquale E, Cacciatore C, Fabre S. The fundamental role of bone morphogenetic protein 15 in ovarian function and its involvement in female fertility disorders. *Hum Reprod Update*. 2014;20(6):869–883.
17. Hopkins J, et al. Meiosis-specific cohesin component, Stag3 is essential for maintaining centromere chromatid cohesion, and required for DNA repair and synapsis between homologous chromosomes. *PLoS Genet*. 2014;10(7):e1004413.
18. Lutzmann M, et al. MCM8- and MCM9-deficient mice reveal gametogenesis defects and genome instability due to impaired homologous recombination. *Mol Cell*. 2012;47(4):523–534.
19. King RC. The meiotic behavior of the Drosophila oocyte. *Int Rev Cytol*. 1970;28:125–168.
20. Spradling AC. Germline cysts: communes that work. *Cell*. 1993;72(5):649–651.
21. Bione S, et al. A human homologue of the Drosophila melanogaster diaphanous gene is disrupted in a patient with premature ovarian failure: evidence for conserved function in oogenesis and implications for human sterility. *Am J Hum Genet*. 1998;62(3):533–541.
22. Castrillon DH, Wasserman SA. Diaphanous is required for cytokinesis in Drosophila and shares domains of similarity with the products of the limb deformity gene. *Development*. 1994;120(12):3367–3377.
23. Casanueva MO, Ferguson EL. Germline stem cell number in the Drosophila ovary is regulated by redundant mechanisms that control Dpp signaling. *Development*. 2004;131(9):1881–1890.
24. Bui KH, et al. Integrated structural analysis of the human nuclear pore complex scaffold. *Cell*. 2013;155(6):1233–1243.
25. Boehmer T, Jeudy S, Berke IC, Schwartz TU. Structural and functional studies of Nup107/Nup133 interaction and its implications for the architecture of the nuclear pore complex. *Mol Cell*. 2008;30(6):721–731.
26. Whittle JR, Schwartz TU. Architectural nucleoporins Nup157/170 and Nup133 are structurally related and descend from a second ancestral element. *J Biol Chem*. 2009;284(41):28442–28452.
27. Gigliotti S, et al. Nup154, a new Drosophila gene essential for male and female gametogenesis is related to the nup155 vertebrate nucleoporin gene. *J Cell Biol*. 1998;142(5):1195–1207.
28. Senger S, Csokmay J, Akbar T, Jones TI, Sengupta P, Lilly MA. The nucleoporin Seh1 forms a complex with Mio and serves an essential tissue-specific function in Drosophila oogenesis. *Development*. 2011;138(10):2133–2142.
29. Li MA, Alls JD, Avancini RM, Koo K, Godt D. The large Maf factor Traffic Jam controls gonad morphogenesis in Drosophila. *Nat Cell Biol*. 2003;5(11):994–1000.
30. Katsani KR, Karess RE, Dostatni N, Doye V. In vivo dynamics of Drosophila nuclear envelope components. *Mol Biol Cell*. 2008;19(9):3652–3666.
31. Sahai-Hernandez P, Nystul TG. A dynamic population of stromal cells contributes to the follicle stem cell niche in the Drosophila ovary. *Development*. 2013;140(22):4490–4498.
32. Hayashi S, et al. GETDB, a database compiling expression patterns and molecular locations of a collection of Gal4 enhancer traps. *Genesis*. 2002;34(1–2):58–61.
33. Morris LX, Spradling AC. Long-term live imaging provides new insight into stem cell regulation and germline-soma coordination in the Drosophila ovary. *Development*. 2011;138(11):2207–2215.
34. Taddei A, et al. Nuclear pore association confers optimal expression levels for an inducible yeast gene. *Nature*. 2006;441(7094):774–778.
35. Terry LJ, Wente SR. Nuclear mRNA export requires specific FG nucleoporins for translocation through the nuclear pore complex. *J Cell Biol*. 2007;178(7):1121–1132.
36. Cautain B, Hill R, de Pedro N, Link W. Components and regulation of nuclear transport processes. *FEBS J*. 2015;282(3):445–462.
37. Liang Y, Hetzer MW. Functional interactions between nucleoporins and chromatin. *Curr Opin Cell Biol*. 2011;23(1):65–70.
38. Capelson M, Liang Y, Schulte R, Mair W, Wagner U, Hetzer MW. Chromatin-bound nuclear pore components regulate gene expression in higher eukaryotes. *Cell*. 2010;140(3):372–383.

39. Blobel G. Gene gating: a hypothesis. *Proc Natl Acad Sci U S A*. 1985;82(24):8527–8529.
40. Vaquerizas JM, Suyama R, Kind J, Miura K, Luscombe NM, Akhtar A. Nuclear pore proteins nup153 and megator define transcriptionally active regions in the Drosophila genome. *PLoS Genet*. 2010;6(2):e1000846.
41. Tan-Wong SM, Wijayatilake HD, Proudfoot NJ. Gene loops function to maintain transcriptional memory through interaction with the nuclear pore complex. *Genes Dev*. 2009;23(22):2610–2624.
42. Oki M, Valenzuela L, Chiba T, Ito T, Kamakaka RT. Barrier proteins remodel and modify chromatin to restrict silenced domains. *Mol Cell Biol*. 2004;24(5):1956–1967.
43. Gomez-Cavazos JS, Hetzer MW. Outfits for different occasions: tissue-specific roles of Nuclear Envelope proteins. *Curr Opin Cell Biol*. 2012;24(6):775–783.
44. Zhang X, et al. Mutation in nuclear pore component NUP155 leads to atrial fibrillation and early sudden cardiac death. *Cell*. 2008;135(6):1017–1027.
45. Basel-Vanagaite L, et al. Mutated nup62 causes autosomal recessive infantile bilateral striatal necrosis. *Ann Neurol*. 2006;60(2):214–222.
46. Grimaldi MR, Cozzolino L, Malva C, Graziani F, Gigliotti S. nup154 genetically interacts with cup and plays a cell-type-specific function during Drosophila melanogaster egg-chamber development. *Genetics*. 2007;175(4):1751–1759.
47. Riparbelli MG, Gigliotti S, Callaini G. The Drosophila nucleoporin gene nup154 is required for correct microfilament dynamics and cell death during oogenesis. *Cell Motil Cytoskeleton*. 2007;64(8):590–604.
48. Huebner A, et al. Mice lacking the nuclear pore complex protein ALADIN show female infertility but fail to develop a phenotype resembling human triple A syndrome. *Mol Cell Biol*. 2006;26(5):1879–1887.
49. Cole F, et al. Homeostatic control of recombination is implemented progressively in mouse meiosis. *Nat Cell Biol*. 2012;14(4):424–430.
50. Bolcun-Filas E, Rinaldi VD, White ME, Schimenti JC. Reversal of female infertility by Chk2 ablation reveals the oocyte DNA damage checkpoint pathway. *Science*. 2014;343(6170):533–536.
51. Palancade B, Liu X, Garcia-Rubio M, Aguilera A, Zhao X, Doye V. Nucleoporins prevent DNA damage accumulation by modulating Ulp1-dependent sumoylation processes. *Mol Biol Cell*. 2007;18(8):2912–2923.
52. De Souza CP, Hashmi SB, Horn KP, Osmani SA. A point mutation in the Aspergillus nidulans sonBNup98 nuclear pore complex gene causes conditional DNA damage sensitivity. *Genetics*. 2006;174(4):1881–1893.
53. Scherthan H, et al. Mammalian meiotic telomeres: protein composition and redistribution in relation to nuclear pores. *Mol Biol Cell*. 2000;11(12):4189–4203.
54. Paulsen RD, et al. A genome-wide siRNA screen reveals diverse cellular processes and pathways that mediate genome stability. *Mol Cell*. 2009;35(2):228–239.
55. Jagot-Lacoussiere L, Faye A, Bruzzoni-Giovanelli H, Villoutreix B, Rain JC, Poyet JL. DNA damage-induced nuclear translocation of Apaf-1 is mediated by nucleoporin Nup107. *Cell*. 2015;14(8):1242–1251.
56. Santos EM, et al. Comparison of three methods of DNA extraction from peripheral blood mononuclear cells and lung fragments of equines. *Genet Mol Res*. 2010;9(3):1591–1598.
57. Rosinger S, et al. Collection and processing of whole blood for transformation of peripheral blood mononuclear cells and extraction of DNA: the Type 1 Diabetes Genetics Consortium. *Clin Trials*. 2010;7(1 suppl):S65–S74.
58. Edgar R, Domrachev M, Lash AE. Gene Expression Omnibus: NCBI gene expression and hybridization array data repository. *Nucleic Acids Res*. 2002;30(1):207–210.
59. Amir el AD, et al. KinSNP software for homozygosity mapping of disease genes using SNP microarrays. *Hum Genomics*. 2010;4(6):394–401.
60. Leinonen R, Sugawara H, Shumway M. The sequence read archive. *Nucleic Acids Res*. 2011;39(Database issue):D19–D21.
61. Li H, Durbin R. Fast and accurate long-read alignment with Burrows-Wheeler transform. *Bioinformatics*. 2010;26(5):589–595.
62. Li H, et al. The Sequence Alignment/Map format and SAMtools. *Bioinformatics*. 2009;25(16):2078–2079.
63. Wang K, Li M, Hakonarson H. ANNOVAR: functional annotation of genetic variants from high-throughput sequencing data. *Nucleic Acids Res*. 2010;38(16):e164.
64. NCBI. dbSNP Short Genetic Variations. NCBI Web site. http://www.ncbi.nlm.nih.gov/SNP/. Accessed September 9, 2015.
65. NHLBI. Exome Variant Server, NHLBI GO Exome Sequencing Project (ESP). NHLBI Web site. http://evs.gs.washington.edu/EVS/. Accessed September 9, 2015.
66. Adzhubei I, Jordan DM, Sunyaev SR. Predicting functional effect of human missense mutations using PolyPhen-2. *Curr Protoc Hum Genet Chapter*. 2013;Chapter 7:Unit7.20.
67. Kumar P, Henikoff S, Ng PC. Predicting the effects of coding non-synonymous variants on protein function using the SIFT algorithm. *Nat Protoc*. 2009;4(7):1073–1081.
68. Katoh K, Standley DM. MAFFT multiple sequence alignment software version 7: improvements in performance and usability. *Mol Biol Evol*. 2013;30(4):772–780.
69. McGuffin LJ, Bryson K, Jones DT. The PSIPRED protein structure prediction server. *Bioinformatics*. 2000;16(4):404–405.
70. Webb B, Sali A. Comparative protein structure modeling using MODELLER. *Curr Protoc Bioinformatics*. 2014;47:5.6.1–5.6.32.
71. The PyMOL Molecular Graphics System, Version 1.7.4 Schrödinger, LLC.